CRYSTAL GROWTH & DESIGN

Article

pubs.acs.org/crystal

From Nanometer Aggregates to Micrometer Crystals: Insight into the Coarsening Mechanism of Calcite

L. N. Schultz,*[,†] K. Dideriksen,[†] L. Lakshtanov,[†,‡] S. S. Hakim,[†] D. Müter,[†] F. Haußer,[∥] K. Bechgaard,[†] and S. L. S. Stipp[†]

[†]Nano-Science Center, Department of Chemistry, University of Copenhagen, Universitetsparken 5, DK 2100 Copenhagen Ø, Denmark

[‡]Institute of Experimental Mineralogy RAS, 142432 Chernogolovka, Russia

[∥]Beuth Hochschule Berlin, University of Applied Sciences, Luxemberger Strasse 10, 13353 Berlin, Germany

Supporting Information

ABSTRACT: Grain size increases when crystals respond to dynamic equilibrium in a saturated solution. The pathway to coarsening is generally thought to be driven by Ostwald ripening, that is, simultaneous dissolution and reprecipitation, but models to describe Ostwald ripening neglect solid−solid interactions and crystal shapes. Grain coarsening of calcite, $CaCO_3$, is relevant for biomineralization and commercial products and is an important process in diagenesis of sediments to rock during geological time. We investigated coarsening of pure, synthetic calcite powder of sub-micrometer diameter crystals and aged it in saturated solutions at 23, 100, and 200 °C for up to 261 days. Scanning electron microscopy (SEM) and Brunauer−Emmett−Teller (BET) surface area analysis showed rapid coarsening at 100 and 200 °C. Evidence of particle growth at 23 °C was not visible by SEM, but high resolution X-ray diffraction (XRD) data demonstrated steady growth of nanometer crystallites. The results can be described by theory where grains coarsen preferentially by aggregation at early times and high temperatures and by Ostwald ripening at later stages. Crystal form and dimension are influenced by the transition from one growth mechanism to the other. This has been poorly described by mean field coarsening models and offers predictive power to grain coarsening models.

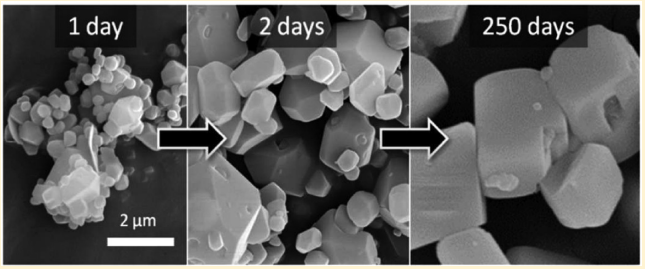

INTRODUCTION

Grain coarsening, first described by Ostwald in 1896,[1] is the tendency for crystals to coarsen during aging in a solution at equilibrium. Grain coarsening can be useful in industrial processes or a nuisance if the application requires constant surface area, particle dimension, or crystal form. When grains dissolve and reprecipitate in a geological formation, the recrystallized portion would have equilibrated with pore fluids, a process that is assumed to be negligible when isotope fractionation is used to make interpretations about paleo-temperature, dating, or the influx of fluids. In all cases where grains coarsen, a robust mechanistic model is central to being able to understand behavior in a crystal−fluid system and to predict its behavior.

Larger crystals are thermodynamically favored over smaller ones, so dynamic equilibrium promotes grain coarsening over time. Surface atoms have fewer solid bonds than those within the bulk, and there are more edge and corner atoms relative to surface atoms on a small crystal than a large one. As a consequence, the contribution of the average surface energy, or the average interfacial tension, $\overline{\gamma}$, is higher for smaller crystals. The solubility near a small particle, $K_{s(A)}$, is higher than the bulk fluid solubility, $K_{s(A=0)}$, as described by a derivative of the Gibbs−Thomson equation (eq 1).[2] This creates a driving force for net ion transport toward the larger particles, where surface area is lower:

$$\log\left(\frac{K_{S(A)}}{K_{S(A=0)}}\right) = \frac{\frac{2}{3}\overline{\gamma}}{3RT}A \qquad (1)$$

Grain coarsening is generally described as Ostwald ripening,[3] that is, dissolution and reprecipitation. However, in systems where the ratio of solid to fluid is high, particles can also grow by aggregation, that is, the formation of larger particles from smaller particles through many possible mechanisms.

Calcite is the most stable form of $CaCO_3$ under most natural conditions. It is present in nearly all geological settings and is a very common industrial mineral. Calcite undergoes grain coarsening during diagenesis of sediments during burial. The degree of diagenesis in an oil-bearing rock is an indicator of porosity and permeability, two important parameters for determining the economic and technical feasibility for oil

Received: September 10, 2013
Revised: December 2, 2013

 © XXXX American Chemical Society dx.doi.org/10.1021/cg401354j | *Cryst. Growth Des.* XXXX, XXX, XXX−XXX

production, such as in the chalk of Northern Europe and Texas. Industries that produce paper, plastics, paint, aspirin tablets, toothpaste, and many other products use calcite as a fine powder, where parameters such as particle size and surface area play an important role in the quality of the product. Thus, better understanding of the controls on calcite crystal coarsening would improve predictive capabilities.

Temperature affects coarsening rates during both Ostwald ripening and growth by aggregation. For Ostwald ripening, the rates of dissolution and precipitation change by Arrhenius dependence and interparticle diffusion changes according to the Stokes–Einstein equation;[4] that is, the diffusivity of the ions that leave and come to the surface is proportional to the ratio of temperature to viscosity. Interfacial tension is also influenced by temperature,[5] thus affecting Ostwald ripening. Temperature affects the likelihood of particles attaching to each other, that is, aggregating, when they come into contact, which is described by Verwey and Overbeek[6] as part of the Derjaguin, Landau, Verwey, Overbeek (DLVO) theory. Attachment is likely to enhance overgrowth when attached particles grow at different rates. If particles do not attach, a growing particle can exert a force on a neighboring particle, thus pushing it away and decreasing the likelihood of overgrowth or encapsulation.

Lifshitz and Slyozov[7] and Wagner[8] first described the mathematics of Ostwald ripening in 1961. Their conclusions, referred to as "LSW theory", still form the cornerstone of our understanding. They determined that a unique and asymptotic particle size distribution is formed in a dilute system of coarsening particles. The predicted "LSW distribution"[3,9] is skewed toward larger values and remains unchanged when normalized to the average radius (i.e., self-similar). Because the breadth of the particle size distribution shows the ensemble driving force for Ostwald ripening, a self-similar distribution allows for a mean field rate description, which can be generalized to any starting material. Once the LSW distribution is established ($t \geq 0$), the average particle radius, $\bar{R}$, grows by a power law dependence:

$$\bar{R}^n(t) - \bar{R}^n(0) = k_{OR}t \quad (2)$$

The rate constant, k_{OR}, depends on many system parameters. The exponential factor, n, is 3 for a diffusion limited system and 2 for a reaction limited system. Because very few experimentalists have collected data that fits an LSW distribution, many recent models have adjusted the parameters in k_{OR}, to achieve a better fit. These models, described in reviews by Voorhees[10] and Baldan,[9] all assume self-similar particle size distributions (i.e., late stage coarsening), isometric particle shapes, and constant interfacial tension. These assumptions are reasonable for some materials, but they describe most real mineral systems poorly.

At high solid to solution ratios, the diffusive field becomes more complex, and one must also consider growth by particle aggregation. Smoluchowski[11] proposed the first theory of rapid particle aggregation. This type of growth was recently observed by Huang et al.,[12] as a precursor to Ostwald ripening in nanocrystalline ZnS. This transitional regime is particularly important for natural mineral systems because solid volume fractions are high and particle size distributions are more often skewed toward smaller values.[13]

A complete description of calcite coarsening ought to improve current models by incorporating crystal growth mechanisms, anisotropic crystal shapes and interfacial tension, higher volume fractions, and evolving particle size distributions. Few, if any, laboratory studies have shown visible calcite coarsening because the rates are slow at low temperatures, especially when particles are large. In this paper, we present results from studies where we synthesized our own pure, submicrometer calcite that we aged in saturated solutions at 23, 100, and 200 °C (i) to observe grain coarsening and particle size distribution changes over time, (ii) to determine if a self-similar particle size distribution is achieved and Ostwald ripening models are applicable, and (iii) to compare the data to a theoretical temperature-dependence based on normal crystal growth and growth by aggregation.

EXPERIMENTAL DETAILS

Calcite Coarsening at High Temperature. Calcite was synthesized by the method described by Schultz et al.,[14] which produces pure material, with particles that are <1 μm in diameter, with surface area that is >10 m^2/g. This method was used because previous experiments (Supporting Figure S1, Supporting Information) showed that coarsening could not be observed using commercial calcite powder (Merck, 99.95 Suprapure) where crystal diameter was initially >10 μm, even at 200 °C.

The calcite-equilibrated aging solution was prepared with 0.1 M NaCl (to maintain constant ionic strength) and an excess (1 g/L) of calcite. After two weeks of stirring at room temperature, the solids were removed by three successive periods of centrifugation for 2 min at 1620*g*. The calcite-equilibrated supernatant was used for all experiments. This solution is henceforth referred to as the equilibrated solution, EQSOL.

We aged calcite samples at 23, 100, and 200 °C. For each sample, time, and temperature in the experiment matrix, 120 mg of calcite were placed into a 1.5 mL polytetrafluoroethylene centrifuge tube with 1 mL of EQSOL. The tubes were sealed and placed into a stainless steel high pressure/temperature reactor (Parr Instruments, model 4923EE), surrounded by EQSOL, and the vessel was heated to the target temperature. Periodically, for up to 261 days, samples were removed and centrifuged, and the solids were freeze-dried and then analyzed.

We did not rinse the solid because we did not want to risk changing it. From its porosity (~30%), we estimated that <50 μL of EQSOL remained in the solid pellet after centrifugation. When the water evaporated, this amount would produce 0.29 mg of NaCl, that would add <0.25% to the solid mass after drying, which is negligible. The reactor pressure was the vapor pressure of EQSOL, that is, ~16 bar for experiments at 200 °C and ~1 bar for those at 100 °C. We assumed that the effect of pressure on coarsening in an incompressible fluid is negligible compared to the effect of temperature. Also, as temperature increases, the solubility of calcite decreases because of the decreased solubility of CO_2, that is, decreased activity of the carbonate species.[15] Thus, heating EQSOL from laboratory temperature, 23 °C, to 200 °C could result in a maximum of 2.3 μg of calcite precipitated, or <0.002% of the sample mass, which is also negligible.

Particle Analyses. Dried samples were mounted on aluminum sample stubs, coated with ~10 nm of gold and imaged with scanning electron microscopy (SEM; FEI Quanta 3D). To measure particle size distribution at each sample time, we selected a representative SEM image containing at least 150 particles. A polygon selection tool in the ImageJ software[16] was used to outline the two-dimensional profile of each particle. The cross sectional area was quantified, and the diameter for each particle was estimated by assuming a spherical shape. For the equant rhombohedral crystal form of calcite, this is a reasonable assumption.

We used the Brunauer–Emmett–Teller method (BET)[17] to measure the specific surface area of the dried calcite samples (Quantachrome, Nova 2000). X-ray diffraction (XRD) was used to confirm calcite purity and to observe changes in crystal size that could not be resolved with SEM or BET. XRD was done using a Bruker Advanced diffractometer (Discover D8) with Cu radiation with Kα1 (λ = 1.5406 Å) and Kα2 (λ = 1.5445 Å) over the 2θ range from 5° to 90°. The fwhm broadening of the Bragg peaks, when calibrated and

dx.doi.org/10.1021/cg401354j | Cryst. Growth Des. XXXX, XXX, XXX–XXX

compared with a LaB_6 standard, provides crystallite dimension from the Scherrer formula.[18] Phase identification and fwhm determination were made using the TOPAS 4.2 software package.

RESULTS AND DISCUSSION

Surface Area and Crystal Size. The surface area of the calcite used for all of the experiments was initially 11.8 m^2/g. Figure 1 shows a clear decrease in surface area with time during reaction at 100 and 200 °C. At room temperature, there is no change within BET analytical uncertainty (10%).

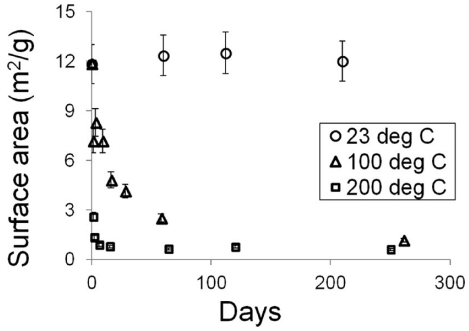

Figure 1. Evolution of calcite surface area as it aged at 23, 100, and 200 °C. Error bars show uncertainty (10%) in the BET method.

XRD of the starting material confirmed that calcite was the only solid phase present (Supporting Figure S2, Supporting Information). Although no changes were observed with SEM or BET for the samples aged at 23 °C, Rietveld refinement of the XRD patterns showed that crystallite dimensions on each face grew steadily (Table 1). The specific numbers recorded in the table cannot be assumed to represent the absolute particle size because the Sherrer equation is only applicable for nanometer-scale crystals. However, the trends in the data indicate crystallite growth. For the sample at 210 days, and for all the samples aged at 100 and 200 °C, the crystallite diameters were too large for effective application of the Rietveld method. XRD data have been averaged for the entire particle volume but growth would have occurred near the reactive interface. Therefore, growth would decrease the interfacial tension by removing surface defects and indicate coarsening.

Table 1. Crystallite Dimensions[a] over Time, for Samples Aged at 23 °C, for the Major Calcite Crystal Faces

crystal face	{01.2}	{10.4}	{11.0}	{11.3}	{20.2}
0 days	217	157	84	80	76
60 days	264	205	131	103	113
112 days	465	304	158	129	163

[a]In nanometers.

SEM Image Analysis. No visible changes could be seen in the SEM images for samples aged at 23 °C (Supporting Figure S3, Supporting Information), but clear changes were seen for samples aged at 100 and 200 °C. Calcite particles coarsened after only one day at 200 °C, and many grew to diameters of 2 μm or more after 2 days (Figure 2). The larger particles grew rapidly for the first 15 days, and the smaller particles either dissolved or were engulfed by larger, growing crystals. The engulfing process is most evident in the image at 2 days, where small windows in the large crystal allow the engulfed particles to be seen. At this stage in the experiment, coarsening rates were fast, and sub-micrometer particles remained in close proximity to the larger, growing crystals.

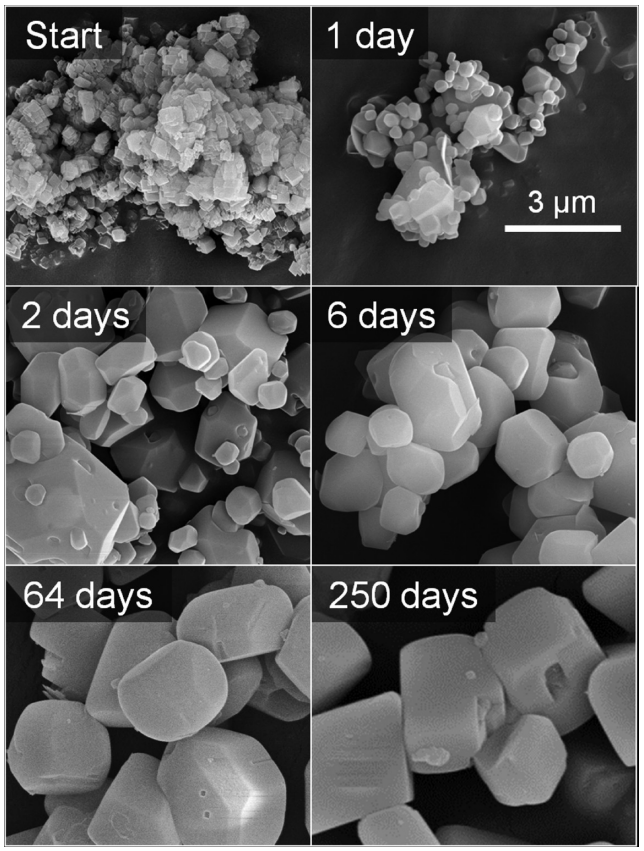

Figure 2. SEM images of calcite coarsening at 200 °C. The scale bar is the same for all images. Days 15, 29, and 120 are not shown, but they can be seen in Figure S4 in the Supporting Information.

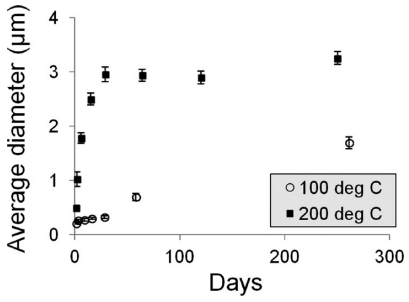

Figure 3. Average diameter of particles that coarsened at 100 and 200 °C. Error bars show the 95% confidence interval of the mean estimates based on counting over 150 particles for each sampling time.

After 1 day, the particle size distribution was skewed, with an abundance of small particles (Figure 4, top). Over time, the size distribution evolved to a more symmetric form. The size distribution can also be represented as a cumulative count from the smallest to largest (Figure 4, bottom), which shows a shifting profile that favors larger particles, a growing median diameter, and a larger spread in particle size. The exact images used for the measurements are provided in Supporting Figure S4, Supporting Information.

Compared to data at 200 °C, coarsening at 100 °C was much slower, but effects were evident even after only 1 day of reaction (Figure 5). After 261 days at 100 °C, the average

dx.doi.org/10.1021/cg401354j | Cryst. Growth Des. XXXX, XXX, XXX−XXX

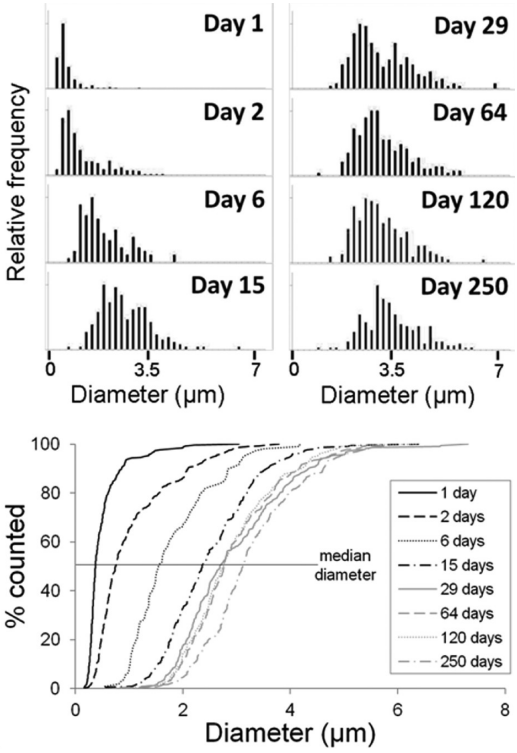

Figure 4. Evolution of the particle size distribution during aging of the fine grained calcite at 200 °C.

diameter was 1.6 μm, compared with 3 μm at 200 °C (Figure 3). Crystal form was generally rhombohedral.

For the samples aged at 100 °C, the particle size distribution (Figure 6) evolved in the same way but at a slower rate. The exact images used for the measurements are provided in Supporting Figure S5, Supporting Information. The particle size distributions at both temperatures demonstrated that neither the LSW distribution nor a self-similar distribution had yet been achieved, and thus the mean field models that assume such profiles (i.e., in the form of eq 2) are not valid.

After 261 days at 100 °C, the distribution is still skewed toward smaller values. The distribution resembles the shape and average radius that was measured after 6 days for samples aged at 200 °C, but the crystal form is much more rhombohedral. This observation is quite interesting because it suggests a different growth mechanism. Behavior could be explained by a difference in surface nucleation and growth or by the influence of aggregation.

At low saturation state, where homogeneous nucleation is highly unlikely, crystals grow mass by spiral growth[19,20] adding material at dislocations and building terraces that expand outward, one by one. Growth rates are controlled by saturation state, solution composition,[21,22] and interfacial tension.[20] Particles were initially rhombohedral, showing exposed {10.4} faces, so if Ostwald ripening (i.e., surface growth) is responsible, the ratio of the velocity perpendicular to the {10.4} face, v_1, to the velocity parallel, v_2, would have to be higher at 200 °C in order to create other exposed faces that did not exist before. Figure 7 shows the similar particle size distributions.

Figure 8 describes how growth rates during spiral growth, v_1 and v_2, could influence which face is expressed.

If crystal face growth explains the difference in crystal form, the final particle size could be determined primarily by the ratio

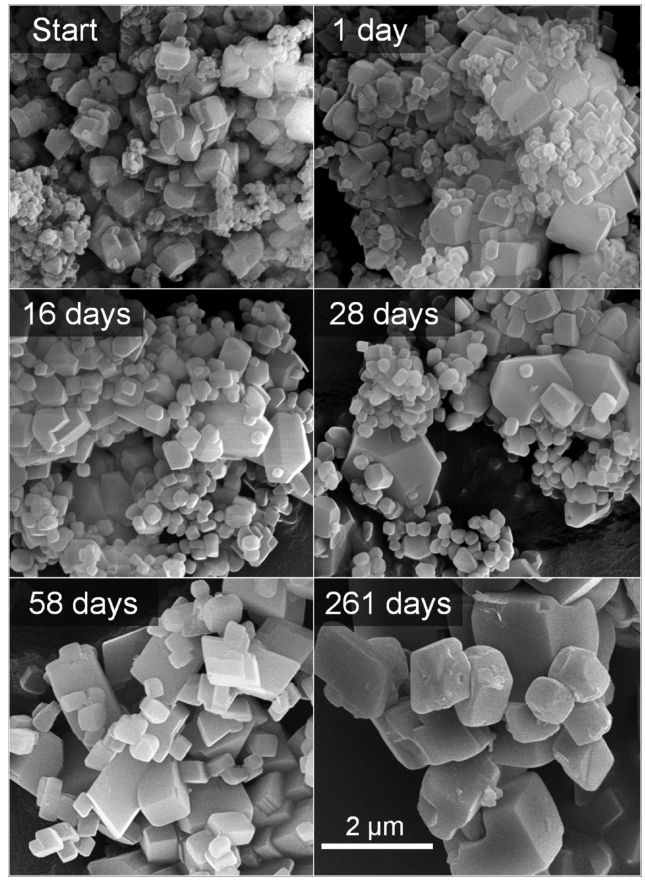

Figure 5. SEM images of calcite coarsening at 100 °C. The scale bar is the same for all images. Days 3 and 9 are not shown, but they can be seen in Supporting Figure S3, Supporting Information.

of v_1 to v_2, and thus temperature. This highlights a behavior unique to mineral systems that current Ostwald ripening models do not consider but that could have important effects on long-term prediction of particle coarsening at different temperatures.

Comparison of Experimental Rates with Theoretical Estimates at 100 and 200 °C. In this section, we estimate the theoretical ratio between calcite growth rate (dr/dt) at 200 and 100 °C. In the first case, we assume that growth occurs by Ostwald ripening, that is, normal crystal growth. In the second case, we assume that particles grow by aggregation. It is likely that both mechanisms contribute to total coarsening in the experimental systems. The purpose of the theoretical estimates is (i) to see if we should expect more growth by aggregation, relative to Ostwald ripening, at 200 °C, which could explain why the particle shapes are different and there is more encapsulation at 200 °C in Figure 7, and (ii) to see if the temporal change in experimental growth rate ratios (i.e., Figure 3) suggests that the mechanism changes over time.

If we consider only the first four points at 200 °C, where the final particle sizes after 6 days are similar to the final particle sizes at 100 °C after 261 days, we see that the ratio, $(dr/dt)_{200}/(dr/dt)_{100}$, is approximately 27 (plots are presented in Supporting Figure S6, Supporting Information). In the same data range, the ratio of dr^2/dt is 42, which is more convenient for comparison with the theoretical model for growth by aggregation. The ratio, $(dr/dt)_{200}/(dr/dt)_{100}$, decreases over time.

dx.doi.org/10.1021/cg401354j | Cryst. Growth Des. XXXX, XXX, XXX−XXX

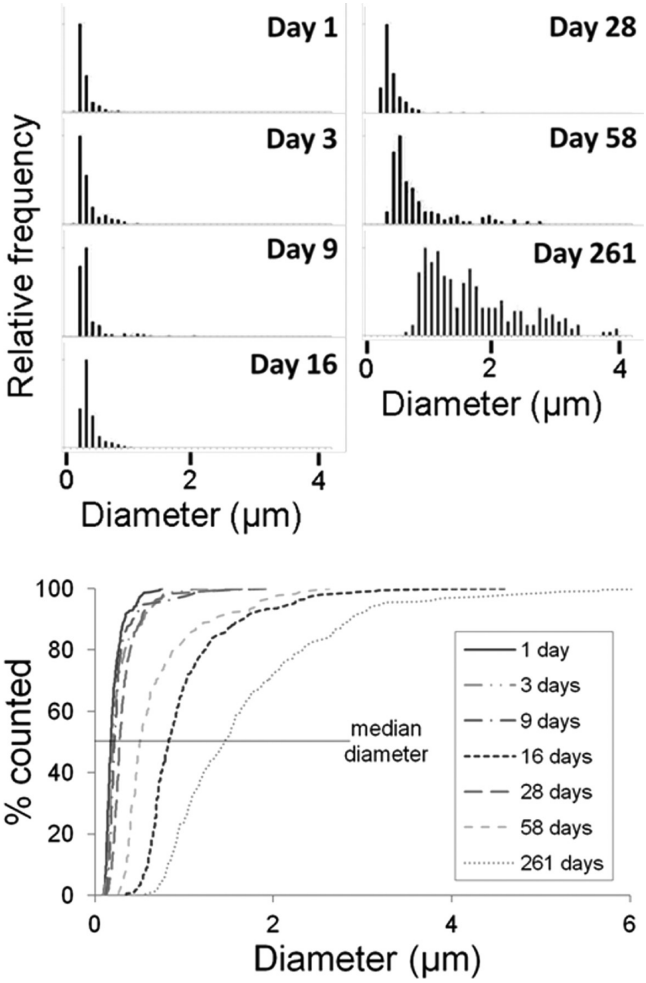

Figure 6. Particle size distributions of calcite exposed to 100 °C.

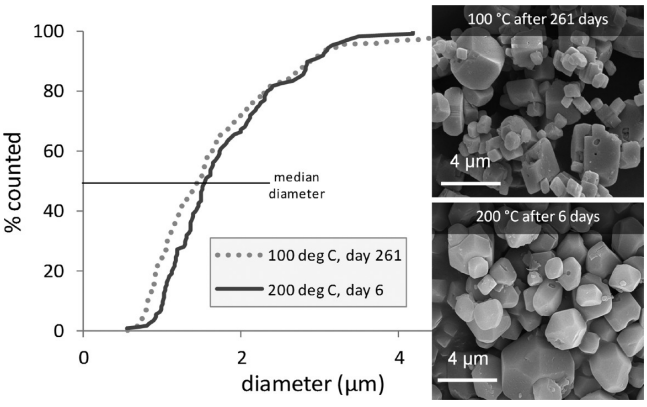

Figure 7. Cumulative distribution after 261 days at 100 °C and 6 days at 200 °C, showing similarity in size and distribution in spite of a difference in crystal form (inset images).

Growth by Ostwald Ripening. If Ostwald ripening dominates and if we assume equal molar concentrations (i.e., $C = [Ca^{2+}] = [CO_3^{2-}]$), normal calcite growth can be described by eq 3, where r represents the radius, β represents the kinetic coefficient, K_s is the solubility of calcite ($10^{-9.27}$ at 100 °C and $10^{-11.29}$ at 200 °C),[15] and f_2 is the divalent ion activity coefficient:[19]

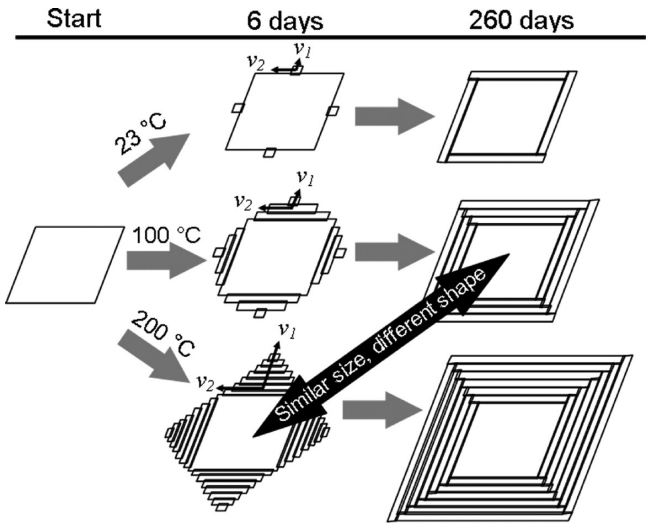

Figure 8. Drawing that describes how crystal faces might grow at the three temperatures. The flat surfaces represent the {10.4} face of calcite, and the growth velocities, v_1 and v_2, represent growth perpendicular and parallel to this face.

$$\frac{dr}{dt} = \beta\left(C - \frac{K_S^{1/2}}{f_2}\right) \tag{3}$$

Equation 3 can be rewritten using the Gibbs–Thompson equation, relating concentration, C, to molar volume, V_m, interfacial tension, γ, and radius, r:

$$\frac{dr}{dt} = \beta\left(\frac{K_S^{1/2}}{f_2}\frac{2\gamma V_m}{rRT}\right) \tag{4}$$

To relate β to T, an apparent activation energy of ~46 kJ/mol has been estimated by several researchers.[23−26] One higher value (155 kJ/mol) was estimated by Koutsoukos and Kontoyannis,[27] who were the only ones to study crystals immediately after nucleation. Using 46 kJ/mol, we estimate that the ratio, β_{200}/β_{100}, is 23 based on Arrhenius dependence; that is, $\beta \propto \exp(E_a/RT)$. A reasonable γ for calcite in aqueous NaCl solution is 98 mJ/m^2, determined by Sohnel.[5] Nothing is known about the temperature dependence of γ for calcite, but we can relate γ to the equilibrium concentration, C_0, (from K_s at 100 and 200 °C)[15] by an empirical correlation:[28]

$$\gamma\left(\frac{mJ}{m^2}\right) = -18.3 \log C_0 + 34.5 \tag{5}$$

From this we estimate that γ_{200} = 138 mJ/m^2 and γ_{100} = 119 mJ/m^2. Finally, we can estimate f_2 using the Davis equation: For calcite in 0.1 M NaCl, f_2 = 0.33 at 100 °C and f_2 = 0.23 at 200 °C. Going back to eq 4, we can now estimate that for Ostwald ripening, $(dr/dt)_{200°C}/(dr/dt)_{100°C} \approx$ **3.3**.

This estimate is an order of magnitude smaller than the data for the first four time points, that is, when most coarsening occurred, but is closer to the total growth at the end points of the experiment, namely, 1.9.

Growth by Aggregation. For an estimate, we use the theory of rapid aggregation by Smoluchowski.[11] From this, it can be shown that particle growth is estimated by[29,30]

$$r_1^2 - r_0^2 = \frac{1}{3}\frac{n_\infty RT}{A\eta W r_2}t \tag{6}$$

dx.doi.org/10.1021/cg401354j | Cryst. Growth Des. XXXX, XXX, XXX−XXX

where n_∞ is the bulk concentration of the subparticles, r_1 is the radius of the primary particle, r_0 is the radius of the primary particle at $t = 0$, r_2 is the radius of the subparticle, A is Avogadro's number, η is the medium viscosity (0.25 cP at 100 °C and 0.05 cP at 200 °C),[31] and W is the stability (or Fuchs) factor. If $W = 1$, then everytime two particles collide, they remain attached. If we assume that the particles attach side by side, we can assume that they approach each other as parallel plates[32] and estimate W by

$$W = \frac{1}{2\kappa d}\exp\left(\frac{E_m}{RT}\right) \quad (7)$$

where κ^{-1} represents the Debye length and d is the half distance between plates. E_m can be estimated with DLVO theory[6] as the maximum of the interparticle potential function $V = V_R + V_A$, where V_R and V_A represent the repulsive and attractive potentials, given by

$$V_A = \frac{AO}{48\pi d^2} \quad (8)$$

$$V_R = 2000/RT\kappa^{-1}O\left(\frac{f\psi}{RT}\right)(1 - \tanh \kappa d) \quad (9)$$

A is the Hamaker constant (10^{-20} J for calcite),[33] O represents the area of surface interaction (9×10^{-15} m^2), which we estimated to be the square of the initial particle radius obtained from the measured surface area. I represents ionic strength (0.1 M), F is the Faraday constant, and ψ is the diffuse layer potential, which is assumed to be the ζ-potential. Calcite data for ζ-potential are numerous and controversial[34] because the value depends on pH, pCO_2, pCa, ionic strength, and saturation state. For estimating, we assumed 25 mV, which is close to the values measured for calcite in 0.1 M NaCl by Nyström et al[35] and Eriksson et al.[36]

For 25 °C, the interparticle potential function, V, is calculated to be 100 (in kT units). At 100 °C, $V = 3$ and at 200 °C, there is no maximum. This is important because it implies that at 25 °C, the potential barrier for aggregation is high so the suspension is stable and the particles are more likely to coarsen by Ostwald ripening. We can now calculate from eq 7 that $W_{100°C} = 90$ and $W_{200°C} = 1$ and then use these values to estimate (dr^2/dt). We used the square of the radius for comparison with eq 6. For growth by aggregation, $(dr^2/dt)_{200°C}/(dr^2/dt)_{100°C} \approx$ **570**.

We note that this estimate is for illustrative purposes only, mainly because of uncertainty in ζ-potential and its temperature dependence and the assumption that Ca^{2+} and CO_3^{2-} activities are equal. If we alternatively assume a ζ-potential of 15 mV or less, then $W_{100} \approx W_{200}$ and the rate ratio reaches a minimum of 6.3 (i.e., the ratio of other parameters in eq 6). If we assume a ζ-potential of 30 mV, then $W_{100°C} \gg W_{200°C}$, and the rate ratio is 3×10^4. Even at the minimum, the ratio estimate is greater for growth by aggregation than for Ostwald ripening, and it could potentially be orders of magnitude stronger for higher, more reasonable ζ-potential estimates. The higher estimate could also explain why Koutsoukos and Kontoyannis[27] estimated an unusually high E_a for small calcite particles: The growth was likely influenced by aggregation.

CONCLUSIONS

This study demonstrates that grain coarsening of calcite at 100 and 200 °C is characterized in the early stages by fast growth of particles by aggregation. As time proceeds, less stable faces are eliminated, and the thermodynamically favored rhombohedral form returns. Temperature influenced not only the rates but also the mechanism of growth. This conclusion is supported by a theoretical comparison of rates, which highlights a strong temperature dependence of the stability factor W. When combined with the observation of encapsulation at early stages, and most notably in the experiments at 200 °C, this provides strong evidence that the early stages grew by aggregation, and the late stages were dominated by Ostwald ripening. A similar observation, where ZnS nanoparticles coarsened by oriented attachment, followed by Ostwald ripening, was reported by Huang et al.[12] Our results suggest that a similar transition occurs with the slower coarsening rates of calcite if particles are small and temperature is high.

Grain coarsening at 23 °C could not be proven by data from BET or SEM, but estimates of crystal face dimensions using Rietveld refinement of high resolution XRD data provide clear evidence that crystallites grew steadily from 0.4 to 2.2 nm/day along each crystal axis. This demonstrates that even at slow rates and at a temperature with a high energy barrier for aggregation, the surfaces continue to rearrange and grow. This is Ostwald ripening, and the process affects average interfacial tension by eliminating kinks and steps.

Traditional mean-field Ostwald ripening models poorly describe behavior in systems with high solid to fluid ratios, evolving particle size distributions, and particle aggregation, but these qualities are very relevant in real systems. For example, diagenesis in sedimentary basins and coarsening in industrial pastes occur at high solid to liquid ratios, and the particle size distributions are most commonly skewed to the right.[13] Thus in summary, our results demonstrate that for systems at elevated temperatures or high solid to fluid ratios, including the effects of particle aggregation and a dynamic and anisotropic interfacial tension results in a more realistic model to describe grain coarsening.

ASSOCIATED CONTENT

Supporting Information

Six additional figures. This material is available free of charge via the Internet at http://pubs.acs.org.

AUTHOR INFORMATION

Corresponding Author

*Address: Nano-Science Center, Department of Chemistry, University of Copenhagen, Room C-114, Universitetsparken 5, DK 2100, Copenhagen Ø, Denmark. E-mail: lschultz@nano.ku.dk. Phone: (+45 35320223).

Notes

The authors declare no competing financial interest.

ACKNOWLEDGMENTS

We thank K. West and F. Engstrøm for discussions, F. Shadab for laboratory assistance, and J. D. Rodriguez-Blanco for help with XRD interpretation. Funding was provided mostly by the Nano-Chalk Venture, supported by the Danish National Advanced Technology Foundation (HTF), and Maersk Oil and Gas A/S. Minor support came from the UK Engineering and Physical Sciences Research Council (EPSRC, EP/IOO1514/1) through the MIB (Biomineralisation) Project and from the European Community for the Min-Gro Network

(MRTN-CT-2006-035488) and the CarbFix Project (Grant No: FP7-283148).

REFERENCES

(1) Ostwald, W. *Lehrbuch der Allgemeinen Chemie*; Leipzig, Germany, 1896; Vol 2.
(2) Stumm, W.; Morgan, J. J. *Aquatic Chemistry*; John Wiley & Sons, New York, 1996; p 1022.
(3) Voorhees, P. W. *J. Stat. Phys.* **1985**, *38* (1−2), 231−252.
(4) Edward, J. T. *J. Chem. Educ.* **1970**, *47* (4), 261.
(5) Söhnel, O.; Mullin, J. W. *J. Cryst. Growth* **1982**, *60* (2), 239−250.
(6) Verwey, E. J. W.; Overbeek, J. T. G. *J. Polym. Sci.* **1999**, *4* (3), 413−414.
(7) Lifshitz, I.; Slyozov, V. *J. Phys. Chem. Solids* **1961**, *19* (1−2), 35−50.
(8) Wagner, C. *Z. Elektrochem.* **1961**, *65* (7−8), 581−591.
(9) Baldan, A. *J. Mater. Sci.* **2002**, *37* (11), 2171−2202.
(10) Voorhees, P. W. *Annu. Rev. Mater. Sci.* **1992**, *22*, 197−215.
(11) Smoluchowski, M. *Physik. Zeit.* **1916**, *17*, 557−571.
(12) Huang, F.; Zhang, H. Z.; Banfield, J. F. *Nano Lett.* **2003**, *3* (3), 373−378.
(13) Eberl, D. D.; Kile, D. E.; Drits, V. A. *Am. Mineral.* **2002**, *87* (8−9), 1235−1241.
(14) Schultz, L. N.; Andersson, M. P.; Dalby, K. N.; Okhrimenko, D. V.; Fordsmand, H.; Stipp, S. L. S. *J. Cryst. Growth* **2013**, *371*, 34−38.
(15) Plummer, L. N.; Busenberg, E. *Geochim. Cosmochim. Acta* **1982**, *46* (6), 1011−1040.
(16) Rasband, W. S. *ImageJ*; U. S. National Institutes of Health: Bethesda, Maryland, USA, 1997−2013.
(17) Brunauer, S.; Emmett, P. H.; Teller, E. *J. Am. Chem. Soc.* **1938**, *60*, 309−319.
(18) Guinier, A. *X-Ray Diffraction: In Crystals, Imperfect Crystals, and Amorphous Bodies*; W.H. Freeman Company: San Francisco, USA, 1994.
(19) De Yoreo, J. J.; Vekilov, P. G. *Biomineralization* **2003**, 54.
(20) Chernov, A. A. *Usp. Fiz. Nauk* **1961**, *73* (2), 277−331.
(21) Larsen, K.; Bechgaard, K.; Stipp, S. L. S. *Geochim. Cosmochim. Acta* **2010**, *74* (2), 558−567.
(22) Larsen, K.; Bechgaard, K.; Stipp, S. L. S. *Geochim. Cosmochim. Acta* **2010**, *74* (7), 2099−2109.
(23) Inskeep, W. P.; Bloom, P. R. *Geochim. Cosmochim. Acta* **1985**, *49* (10), 2165−2180.
(24) Cassford, G. E.; House, W. A.; Pethybridge, A. D. *J. Chem. Soc., Faraday Trans.* **1983**, *79*, 1617.
(25) Gutjahr, A.; Dabringhaus, H.; Lacmann, R. *J. Cryst. Growth* **1996**, *158* (3), 296−309.
(26) Nancollas, G.; Reddy, M. M. *J. Chem. Soc. Faraday, Trans.* **1971**, *118* (8), C216.
(27) Koutsoukos, P. G.; Kontoyannis, C. G. *J. Chem. Soc., Faraday Trans.* **1984**, *80*, 1181−1192.
(28) Söhnel, O. *J. Cryst. Growth* **1982**, *57* (1), 101−108.
(29) Philipse, A. P. *Colloid Polym. Sci.* **1988**, *266* (12), 1174−1180.
(30) Fuchs, N. Z. *Z. Phys.* **1934**, *89*, 736−743.
(31) McCabe, W. L.; Smith, J. C.; Harriott, P. *Unit Operations of Chemical Engineering*; McGraw-Hill: New York, 2005; Vol. 7.
(32) Overbeek, J. T. G. In *Colloid Science*; Kruyt, H. R., Eds.; Elsevier: Amsterdam, 1960.
(33) Lomboy, G.; Sundararajan, S.; Wang, K.; Subramaniam, S. *Cem. Concr. Res.* **2011**, *41* (11), 1157−1166.
(34) Stipp, S. L. S. *Geochim. Cosmochim. Acta* **1999**, *63* (19−20), 3121−3131.
(35) Nystrom, R.; Linden, M.; Rosenholm, J. B. *J. Colloid Interface Sci.* **2001**, *242* (1), 259−263.
(36) Eriksson, R.; Merta, J.; Rosenholm, J. B. *J. Colloid Interface Sci.* **2007**, *313* (1), 184−193.